Rubbery and Rigid Particle Toughening of Epoxy Resins

B. GEISLER and F. N. KELLEY*

University of Akron, College of Polymer Science and Polymer Engineering, Akron, Ohio 44325-3909

SYNOPSIS

Four types of materials were evaluated in this study: neat epoxy resins of differing initial molecular mass, and their rubbery particle-filled, rigid particle-filled, and hybrid particle-filled counterparts. Both rubbery and rigid particle-filled epoxies exhibited fracture energies, G_{Ic}, greater than the neat resins. Cured resins prepared with an optimum loading of both rubbery and rigid particles gave G_{Ic} values greater than those from rubbery or rigid particles alone (approximately sixteen-fold increase over the neat resins). Rigid particle composites were toughened by means of a crack front impedance mechanism. In hybrid particle composites, rigid particles enhanced localized plastic deformation ahead of the crack front.

INTRODUCTION

Epoxy resins have long been used in applications such as adhesives, electronics encapsulation, and as the matrix material for continuous filament laminates. Cured epoxy resins have desirable properties such as high modulus, creep resistance, and good elevated temperature properties. Unfortunately, unmodified epoxies are often brittle and show poor resistance to crack propagation. Increasing the ductility of the matrix resin increases its cohesive fracture energy. However, this increase is not observed in matrix-dominated fracture in high fiber content composite laminates, nor for thin-layer adhesives.

The strength of continuous filament epoxy composites is controlled by three factors—the properties of the filaments, the nature of the filament/matrix interface, and the matrix material itself. In many instances, failure of a fiber-reinforced laminate occurs within the matrix. Therefore, a detailed understanding of cohesive failure in an adhesive epoxy layer is desirable. Various schemes have been proposed over the last 3 decades to increase the toughness of epoxy matrices. These include alteration of the constituent resin molecules and the inclusion of fillers of assorted physical and chemical character.[1-8] The primary objective of the current work was to establish the efficacy of rubbery and rigid particles as toughening agents for composite matrix resins.

BACKGROUND

LeMay et al.[9-11] examined the effect of crosslink density on the fracture properties of a series of resins based on diglycidyl ether of bisphenol-A (DGEBA) epoxy resins. The aim of these experiments was to create a series of networks in which crosslink density was varied primarily through stoichiometric end-linking chemistry rather than through nonstoichiometric reactions. Average network molecular weight between crosslinks, M_c, was calculated from measurements of rubbery modulus well above the glass transition temperature, T_g, using the theory of rubber elasticity. A logarithmic plot of LeMay's fracture energy data vs. M_c is given as Figure 1. The relationship is linear with a slope of about 1/2. This result can be written as

$$G_{Ic} = KM_c^{1/2} \quad (1)$$

where K is a constant of proportionality.[9,10]

Hunston et al.[12,13] studied a wide variety of thermoset, thermoplastic, and rubber-toughened thermosets as the matrix materials in unidirectional filament laminates. Fracture experiments were per-

*To whom correspondence should be addressed.

Journal of Applied Polymer Science, Vol. 54, 177-189 (1994)
 CCC 0021-8995/94/020177-13

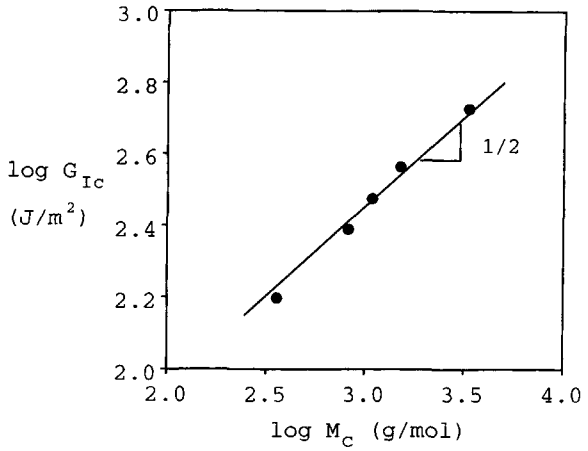

Figure 1 Logarithmic plot of fracture energy, G_{Ic}, vs. molecular weight between crosslinks, M_c, for networks prepared from an homologous series of epoxy resins. (Data from Ref. 11.)

formed with each of the resins, both as bulk materials and as the matrix for fiber-reinforced composites. Laminate fracture experiments were carried out in transverse fracture in order to emphasize matrix failure rather than filament fracture. Brittle resins gave greater fracture energies in the composites than in the bulk. Filament pullout and fiber breakage were thought to be responsible for the increased fracture energy in the brittle composites. On the other hand, ductile matrix polymers showed reduced toughening in fiber laminates in comparison to their bulk specimen counterparts. Constraint of plastic deformation at the crack tip was thought to be the major reason for the lack of translation of bulk resin properties to the laminates in the case of ductile resins. Bradley and Cohen[14] have demonstrated that plastic deformation can extend 3–5 filament diameters beyond the plane of the primary crack front. So for ductile resins, while there is not complete constraint of the plastic zone by adjacent filaments, the size of the process zone is much smaller than is found in fracture of the bulk material.

Particulate fillers have been used in attempts to toughen epoxy matrix resins. The fillers that have been used can be separated into two categories—rubbery and rigid. Rubbery fillers produce enhanced toughness in bulk matrices, which has been explained by the combination of the following toughening mechanisms: shear yielding, cavitation, plastic void growth, and rubber bridging.[15–23] Rigid particle fillers are typically inorganic materials of high modulus and strength such as glass beads, alumina, or silica. Lange[24] proposed crack pinning as the mechanism responsible for the increased toughness found in rigid particle containing epoxy resins. Hybrid particle composites, as employed in this study, are those composites containing both rubbery and rigid fillers. Kinloch[25] examined epoxy resins toughened with carboxyl terminated butadiene-acrylonitrile liquid rubber (CTBN) and glass beads. It was observed that these hybrid particle composites showed greater toughening than composites toughened either with rubbery filler or with rigid particle filler separately.

EXPERIMENTAL

Materials

Epoxy resins from an homologous series of diglycidyl ether of bisphenol-A (DGEBA) were used. The epoxy resins are from the DER® series of resins produced by Dow Chemical Corporation. Attention was focused on two resins in the series—DER 661 ($\langle M_n \rangle \sim 1000$ g/mol) and DER 664 ($\langle M_n \rangle \sim 1800$ g/mol). The crosslinker used in the study was 4,4'-diaminodiphenyl sulfone (DDS). DDS is a nominal tetrafunctional crosslinker with a molecular weight of 248.3 g/mol and a melting temperature range of 175–178°C. The primary crosslinking reaction is the endlinking of epoxy resin molecules through the reaction of epoxide groups with amine hydrogens of DDS. DDS was purchased from Aldrich Chemical Company. The rubbery particles used in the study were Rohm and Haas Company's Paraloid® KM330 core-shell particles. The core of the particles is composed of poly *n*-butyl acrylate rubber and the shell is made of poly methyl methacrylate. Paraloid KM330 is a powder at room temperature, with some aggregates. Upon incorporation into epoxy resins most aggregates break up, with the majority of the particles having sizes on the order of 1 μm. Alcoa A-4000 SG alumina particles were used as the rigid filler in the study. Alumina particle size was measured by way of optical microscopy. The particles used in the study had an average diameter of 3.3 $\pm$ 1.2 μm. All materials were used as received.

Preparation of Networks

Epoxy resin was weighed into a 500 mL or a 1000 mL reaction kettle, depending on the quantity of material to be prepared.

In the case of particle-filled composites, the particles were added to the epoxy resin before heating the kettle. The kettle was fitted with a standard

cover with four ground joint openings, a stirrer bearing, a stir shaft with Teflon blade, a hose adapter, thermometer, electric heating collar, and a stopper. Vacuum was used to remove lower boiling species in the resin. All reactions were carried out with equal stoichiometric amounts of epoxy resin and DDS. The resin was cured for 5 h in a vertical Teflon-coated aluminum mold that had been preheated to 200°C. Aluminum molds were available in this laboratory with gap thicknesses ranging from 2–22 mm with widths and heights of 150 mm. The oven was allowed to slowly cool to room temperature. The recovered plaque was then machined into whatever shape was needed for experimental purposes. Following machining, the test pieces were returned to a preheated 200°C oven. A total of 10 h of postcure under vacuum was followed by slow cooling of the oven to room temperature. The aforementioned cure and postcure schedule was suggested by LeMay.[11]

Characterization of Cured Networks

Dynamic Mechanical Properties

A Polymer Laboratories Mark II Dynamic Mechanical Thermal Analyser (DMTA) was used to evaluate the level of cure of bulk networks. Experiments were carried out at a frequency of 1 Hz over a range of temperature with a heating rate of 2°C/min. A relatively consistent glass transition temperature, T_g, of a given network was taken to be approximately equal to the temperature corresponding to the peak in the tangent δ curve.

Double Torsion Fracture Test

Analysis. Outwater[26] originated the double torsion fracture test. Figure 2(A) shows a double torsion test piece. W is the sample width, t the sample thickness, and t_n the fracture path thickness. A v-groove is machined into the double torsion specimen. The groove runs the length of the test piece and is centered at $W/2$, providing a route for crack propagation through the center of the width of the sample. Figure 2(B) depicts a typical double torsion test setup for three-point loading. The test piece is supported by two cylindrical bars. W_m is the length of the moment arm for one of the test piece halves at the beginning of the fracture test. P is the load applied to the specimen. The load is applied over a precrack through a small loading tup. Figure 2(C) shows a perspective drawing of the double torsion test in three-point loading.

The analysis of the double torsion specimen has been developed from an energy balance approach in terms of compliance as represented by

$$G_c = \frac{P_c^2}{2}\frac{dC}{dA} \tag{2}$$

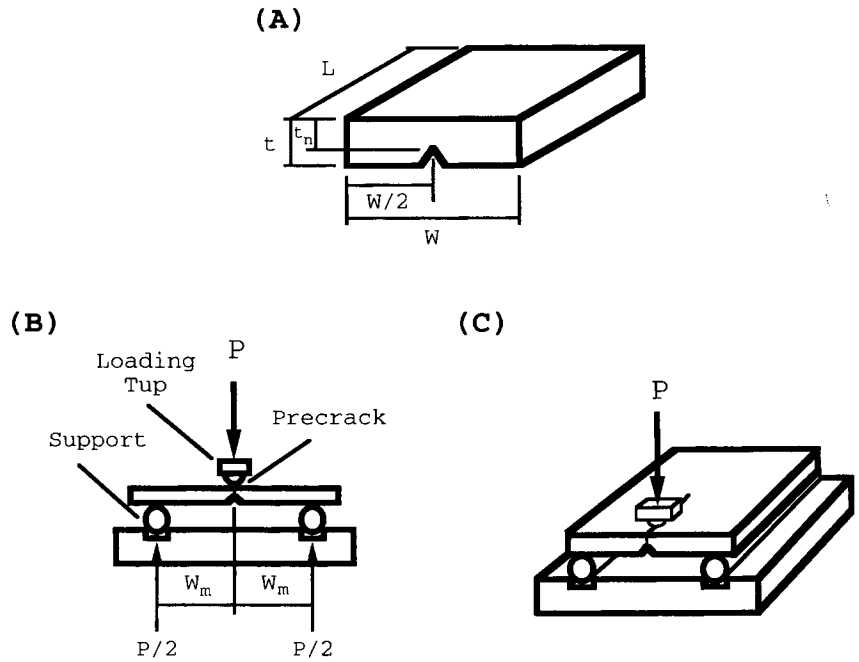

Figure 2 (A) Double torsion test piece. (B) Front view of double torsion fracture test setup. (C) Perspective view of double torsion fracture test.

for linear elastic fracture mechanics (LEFM) conditions.[26–29] Fracture energy, G_c, is given in terms of the critical applied load, P_c, the compliance, C, of the specimen, and A, the area of the fracture surface. The result of the usual double torsion analysis is an expression for the plane strain fracture energy, G_{Ic},

$$G_{Ic} = \frac{3P_c^2 W_m^2}{E(1-\nu)Wt^3 t_n} \tag{3}$$

where E is the Young's modulus of the material under the conditions of the fracture test, and ν is Poisson's ratio.

Several assumptions are normally made in the double torsion analysis, which typically do not apply to the fracture of glassy polymers, and are given below.

Assumption 1—The thickness of the double torsion specimen is much less than its width. In terms of a dimensionless quantity, T, this assumption may be expressed as

$$\left(T \equiv \frac{2t}{W}\right) \ll 1 \tag{4}$$

Assumption 2—The tup displacement, d, during the fracture of the double torsion sample, is very small. In terms of the dimensionless quantity d/W_m, this assumption implies

$$\frac{d}{W_m} \ll 1 \tag{5}$$

Assumption 3—Application of the loads to the double torsion specimen takes place through point loading.

The coupling of assumptions 2 and 3 shows us that the moment arm lengths are taken to be constant and equal to W_m throughout the fracture of the test pieces. Figure 3 shows a schematic of one-half of a double torsion sample undergoing exaggerated four-point loading. An examination of Figure 3 reveals that the assumption of constant moment arm length during fracture is true only for small θ.

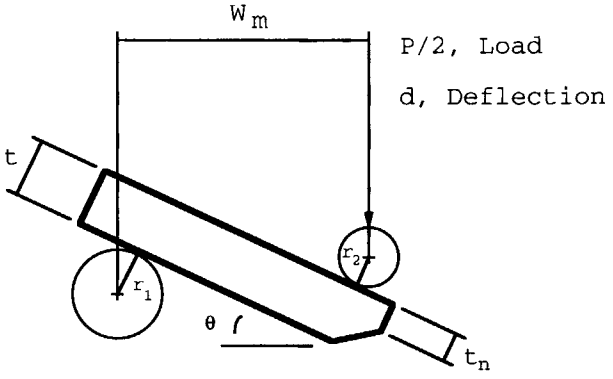

Figure 3 Schematic front view of one-half of a double torsion sample under four point loading.

With the above assumptions in mind, it is apparent that a more rigorous examination is needed for double torsion testing of toughened glassy polymers. If the energy balance is taken in terms of the torsional moment, M, rather than the compliance, then the fracture energy is given by

$$G_c = \frac{M^2}{t_n GK} \tag{6}$$

where G is the shear modulus of the material

$$G = \frac{E}{2(1+\nu)} \tag{7}$$

and K depends on the shape of the bar's cross-section. K is the polar moment of inertia for a circular cross-section. All other cross-sections generate a K that is less than the polar moment of inertia. For a rectangular cross-section, K has been estimated to be[30]

$$K = Wt^3\left[\frac{1}{6} - 0.21\left(\frac{t}{W}\right)\left(1 - \frac{4}{3}\frac{t^4}{W^4}\right)\right] \tag{8}$$

The dimensionless quantity $T = 2t/W$ may be used to give

$$K = \frac{Wt^3}{6}\left[1 - 0.63T\left(1 - \frac{T^4}{12}\right)\right] \tag{9}$$

C_{FT} may be defined as

$$C_{FT} = 1 - 0.63T\left(1 - \frac{T^4}{12}\right) \tag{10}$$

which can be used to reduce Eq. (9) to

$$K = \frac{Wt^3}{6} C_{FT} \tag{11}$$

where C_{FT} can be thought of as a finite thickness correction factor to the original double torsion analysis. Leevers[31] has described the torsional moment for the double torsion test as

$$M = W_m \frac{P}{2}\frac{d}{d\theta}\left(\frac{d}{W_m}\right) \tag{12}$$

which takes into account the change in moment arm length with tup displacement, d. Leevers[31] described d/W_m as

$$\frac{d}{W_m} = \tan\theta - \beta(\sec\theta - 1) \tag{13}$$

where β is defined by

$$\beta \equiv \left[\frac{r_1 + r_2 + t}{W_m}\right] \tag{14}$$

and r_1 and r_2 are the radii of the support and loading tup respectively (see Fig. 3). Equation 13 is used to determine θ from the load-displacement record taken during the fracture test. Equation 13 must be inverted by iteration. Differentiation of Eq. (13) with respect to θ results in

$$\frac{d}{d\theta}\left(\frac{d}{W_m}\right) = \sec^2\theta(1 - \beta\sin\theta) \tag{15}$$

Substitution of Eqs. (7), (11), (12), and (15) into Eq. (6) yields

$$G_c = \frac{3P_c^2W_m^2(1+\nu)}{EWt^3t_n}\left[\frac{\sec^4\theta(1-\beta\sin\theta)^2}{C_{FT}}\right] \tag{16}$$

To make Eq. (16) more wieldy, we can define

$$C_{LD} = \sec^4\theta(1 - \beta\sin\theta)^2 \tag{17}$$

which results in

$$G_c = \frac{3P_c^2W_m^2(1+\nu)}{EWt^3t_n}\left(\frac{C_{LD}}{C_{FT}}\right) \tag{18}$$

for plane stress fracture testing. Figure 4 shows C_{LD} vs. d/W_m curves for several arbitrary selections of β, where C_{LD} can be thought of as a large displacement correction factor to the usual analysis of the double torsion test. Note that for plane strain fracture testing, fracture energy is given by[32]

$$G_{Ic} = \frac{3P_c^2W_m^2}{EWt^3t_n(1-\nu)}\left(\frac{C_{LD}}{C_{FT}}\right) \tag{19}$$

Experimental Method. Fracture tests were carried out with either a table model or a floor model Instron tester, depending of the size and fracture toughness of the samples being evaluated. Sample dimensions of thickness, t, and width, W, were measured prior

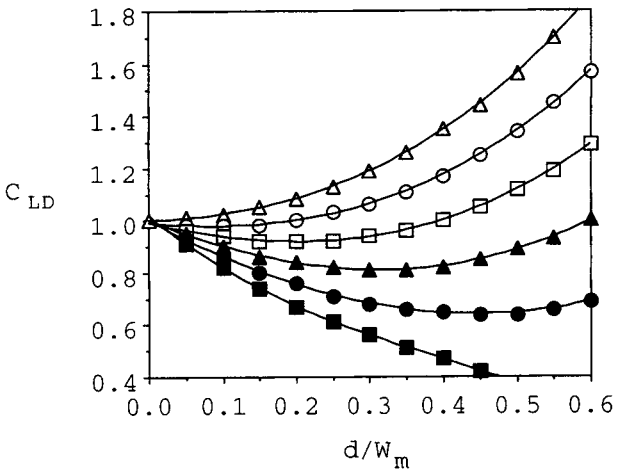

Figure 4 Large displacement correction factor, C_{LD}, vs. d/W_m for a range of β. $\triangle\beta = 0$, $\bigcirc\beta = 0.2$, $\square\beta = 0.4$, $\blacktriangle\beta = 0.6$, $\bullet\beta = 0.8$, $\blacksquare\beta = 1$.

to fracture of the double torsion specimens. A precrack was placed into a double torsion specimen by a rapid blow to a sharp razor blade held over a premachined v-groove at one end of the sample. The double torsion specimen was then placed into a testing jig as shown in Figure 2. Fracture tests were carried out under normal laboratory conditions at a temperature of 23 ± 2°C, with a crosshead speed of 0.05 cm/min. Load-displacement records were taken during the fracture experiments. The load at fracture, P_c, was calculated directly from the data on the load-displacement records. The fracture energies were calculated from Eq. (18) or (19), depending on the conditions of testing. Young's modulus was calculated from near equilibrium three-point bend tests. Poisson's ratio was taken to be 0.35 for all specimens. Because C_{LD} does not vary greatly once crack propagation is underway, it was evaluated at the midpoint of the crack propagation trace.

Three-Point Bend Test

Equilibrium bend tests were carried out on samples from each of the bulk specimens. Samples were loaded by way of a table model Instron in small steps of increasing load. After each incremental loading the load was allowed to decay to a near equilibrium value, P. In addition, the total deflection, d, was tallied during the experiment. A near equilibrium Young's modulus is calculated as[33,34]

$$E = \frac{Pl^3}{4dWt^3} \tag{20}$$

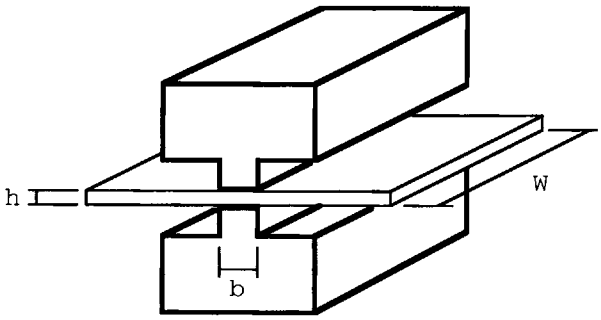

Figure 5 Plane strain compression test.

where it is assumed that the material behaves as a linear elastic solid over the range of deflection. The span between supports is given by l. The width and thickness of the test piece are defined as W and t, respectively. In order to minimize deviation from linear elastic behavior, the total deflection was kept small such that[34]

$$\frac{dt}{l^2} < 0.0008 \tag{21}$$

Plane Strain Compression Test

The plane strain compression test is shown schematically in Figure 5. The width of the test piece is given as W, and the thickness is h_o. The width of the steel dies is b. The plane strain compression test for polymers was first described by Ford and Williams.[35] Ford established that friction effects were minimized with polished die surfaces and with lubricant applied between the die and the specimen.[35] Following the suggestion of Ford and Williams, molybdenum disulfide grease was used as the lubricant in the plane strain compression tests. Load was applied to the specimen with a floor model Instron. A die width of 8 mm was used in the experiments. The resolved equivalent compressive stress, σ, and strain, ε, are given by[35]

$$\sigma = \frac{\sqrt{3}}{2}\frac{P}{W_o b} \tag{22}$$

and

$$\varepsilon = \frac{2}{\sqrt{3}} \ln\left(\frac{h}{h_o}\right) \tag{23}$$

where load is given by P, W_o is the undeformed width of the sample, and h denotes a deformed sample thickness.

RESULTS AND DISCUSSION

Rubbery Particle Optimization

An optimized concentration of rubbery particle filler was determined by conducting fracture tests over a range of filler concentration (0–20 parts per hundred epoxy) for both DER 661 and DER 664. Tables I and II summarize the fracture results for the optimized materials. Fifteen parts per hundred epoxy (phe) Paraloid KM330 gave the greatest increase in K_{Ic} over the neat resin values for both DER 661 and DER 664. However, Young's modulus, E, and compressive yield strength, σ_{yc}, decreased with the addition of rubber filler. The fracture energy is related to fracture toughness as

$$G_c \sim \frac{K_c^2}{E} \tag{24}$$

Because the addition of rubbery filler increases K_{Ic} and decreases E, the result is a dramatic increase in fracture energy at the optimum level of rubber filler loading over G_{Ic} for the corresponding unfilled network. It must be kept in mind that the decrease in Young's modulus when rubber filler is introduced is an undesirable consequence of rubber filler addition, which leads to an increase in fracture energy. Glass transition data are also given in Tables I and II. Note that there was no significant change in apparent T_g of the epoxy networks when rubbery particles were used as filler. The stable T_g is attributed to the use of a core-shell type rubbery filler (rubbery core $T_g \sim -46°C$), which is not expected to undergo

Table I Comparison of Optimized Particle-Filled Composites of DER 661

Paraloid (phe)	Alumina (phe)	K_{Ic} (MPa$\sqrt{m}$)	E (GPa)	G_{Ic} (kJ/m^2)	σ_{yc} (MPa)	T_g (°C)
0	0	0.8 ± 0.1	2.7 ± 0.1	0.2 ± 0.1	95 ± 1	135 ± 2
15	0	2.6 ± 0.2	2.2 ± 0.1	3.1 ± 0.7	71 ± 2	134 ± 2
15	155	3.6 ± 0.2	3.9 ± 0.3	3.3 ± 0.5	101 ± 1	134 ± 2

Table II Comparison of Optimized Particle-Filled Composites of DER 664

Paraloid (phe)	Alumina (phe)	K_{Ic} (MPa$\sqrt{m}$)	E (GPa)	G_{Ic} (kJ/m^2)	σ_{yc} (MPa)	T_g (°C)
0	0	0.9 ± 0.1*	2.8 ± 0.1	0.3 ± 0.1*	87 ± 3	118 ± 2
0	0	1.1 ± 0.2†	2.8 ± 0.1	0.4 ± 0.1†	87 ± 3	118 ± 2
15	0	2.8 ± 0.1	2.1 ± 0.1	3.6 ± 0.3	67 ± 1	118 ± 2
15	100	3.5 ± 0.1	3.6 ± 0.2	3.5 ± 0.4	85 ± 2	119 ± 2

* Denotes arrest value.
† Denotes initiation value.

chemical reaction with epoxy resin during cure. Therefore, the resin is expected to undergo nearly the same network formation reactions regardless of the presences or absence of core-shell rubbery filler during cure.

Figure 6 shows an SEM micrograph of a fracture surface of a rubbery particle toughened DER 664. The composite contained the optimum rubber filler loading of 15 phe. The dark circular regions are cavities which were opened during fracture.

Plane Strain Testing

It has been found in research with metallic materials that the fracture path thickness, t_n, required for plane strain fracture testing can be estimated from[36]

$$t_n \geq 2.5\left(\frac{K_c}{\sigma_{yt}}\right)^2 \tag{25}$$

where σ_{yt} is the tensile value for the yield stress of the material. It is often not possible to determine the tensile yield strength of a brittle epoxy resin under the same conditions as those used in the fracture test. The tensile specimens often fail before significant yielding has been achieved. On the other hand, brittle resins such such as epoxy resins are capable of considerable plastic deformation under compressive loading. Wronski[37] has shown that an estimate of σ_{yt} for epoxy resins can be made based on a measured value of the compressive yield strength, σ_{yc}, of a given resin

$$\sigma_{yt} \approx 0.75\sigma_{yc} \tag{26}$$

Substitution of Eq. (26) into (25) gives

$$t_n \geq 2.5\left(\frac{K_c}{0.75\sigma_{yc}}\right)^2 \tag{27}$$

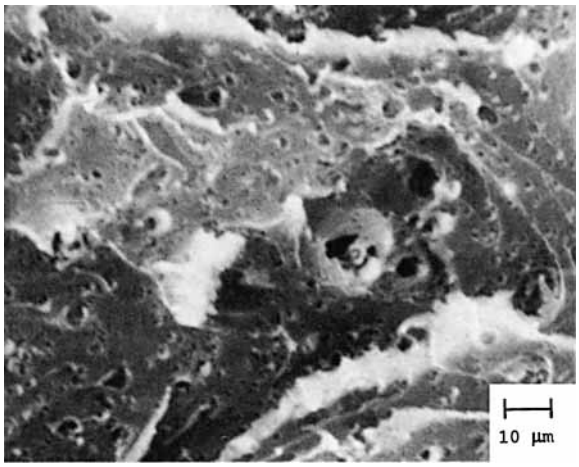

Figure 6 An SEM micrograph of the fracture surface for rubbery particle-toughened DER 664 containing 15 phe Paraloid KM330.

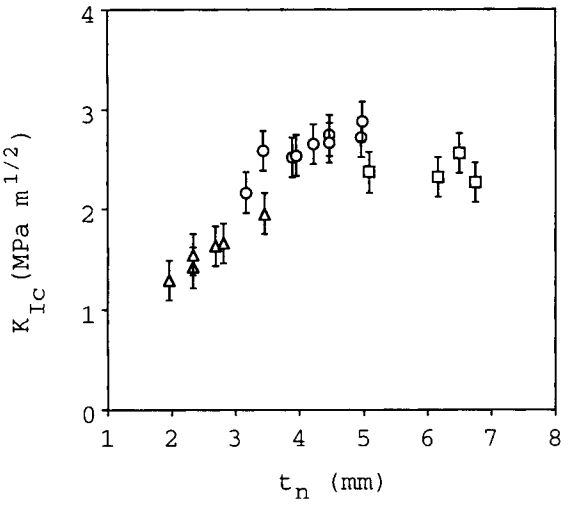

Figure 7 Fracture toughness, K_{Ic}, vs. fracture path thickness, t_n, for DER 661 filled with 15 phe Paraloid KM330. Specimens of varying overall double torsion specimen thickness, t, were used in the fracture experiments Δt = 7 mm, $\circ t$ = 11 mm, $\square t$ = 15 mm.

Table III Specimen Size Effect on G_{IC} (DER 661 Data)

Paraloid (phe)	t Thickness (mm)	t_n Fracture Path Thickness (mm)	Estimated Minimum t_n (mm)	G_{Ic} (kJ/m^2)
0	3.8	2.5	0.3	0.2
15	2.1	1.1	5.9	4.0
15	15.2	6.8	5.9	2.3

Because the compressive yield strength is larger than the tensile yield strength for a given resin, Eq. (27) will give a conservative estimate of the t_n required for plane strain testing. Another, less conservative, estimate of the minimum t_n needed for plane strain fracture testing could be gained from

$$t_n \geq 2.5\left(\frac{K_c}{\sigma_{yc}}\right)^2 \qquad (28)$$

where σ_{yc} is now used to estimate t_n rather than σ_{yt}. It seems reasonable that the estimates of t_n needed for plane strain fracture testing taken from Eqs. (27) and (28) could be used to define a range of t_n in which one would expect the crossover from the plane stress to plane strain condition.

A sample K_c vs. t_n curve for DER 661 filled with 15 phe Paraloid KM330 is given in Figure 7. Using Eqs. (27) and (28) to estimate the crossover region gives an estimated range for t_n of 3.3–5.9 mm. Examining the data in Figure 7 shows that this range fits well to the experimental data. Note that a single specimen size could not be used to investigate the entire t_n range examined in these experiments. Valid double torsion fracture data cannot be obtained when the ratio of t_n to overall specimen thickness is either too small or too large. Further discussion of this point can be found elsewhere.[32]

The data in Table III will be used to compare the fracture energy results of testing in the plane stress region with the plane strain values. The data presented are based on DER 661. Equation 27 was used to estimate the minimum t_n required for plane strain fracture testing. The double torsion fracture test results are given in Table III for three specimens. The neat sample was found to meet the requirements for plane strain fracture testing and gave a G_{Ic} of about 0.2 kJ/m^2. Next, two specimens with 15 phe Paraloid KM330 filler are examined. The first of these rubbery particle filled specimens was tested in the plane stress region and gave a calculated G_{Ic} around 4 kJ/m^2, whereas the other sample was tested in the plane strain region and gave a fracture energy of approximately 2.3 kJ/m^2. The results in Table III demonstrate that the use of an inappropriate fracture test specimen geometry can lead to overestimation of G_{Ic}. It is not uncommon to find values of fracture energy for toughened epoxy in the literature that were taken in the plane stress region, but reported as plane strain, G_{Ic}.

Hybrid Particle Optimization

Hybrid particle composites were optimized on the basis of fracture toughness. Figure 8 shows a plot of fracture toughness, K_{Ic}, vs. volume fraction alumina, V_a, for DER 661 based hybrid particle composites. A constant rubber filler loading of 15 parts per hundred epoxy (phe) was used in these experiments. Initially, little effect on K_{Ic} was found as the volume fraction of alumina was increased. However, there was a change in the manner in which crack propagation takes place for these low volume fractions of

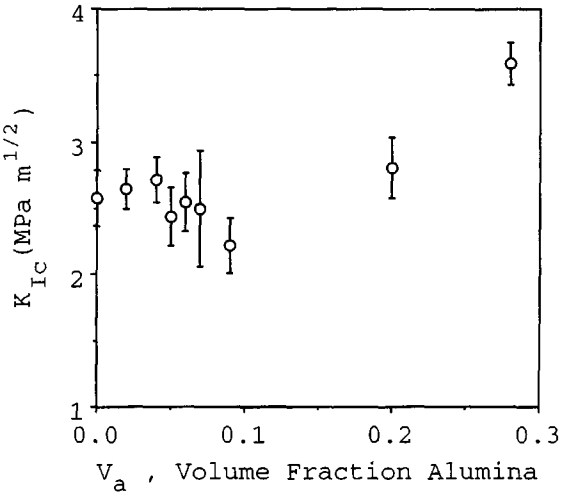

Figure 8 Fracture toughness, K_{Ic}, vs. volume fraction alumina, V_a, for hybrid composites containing 15 phe Paraloid KM330 based on DER 661.

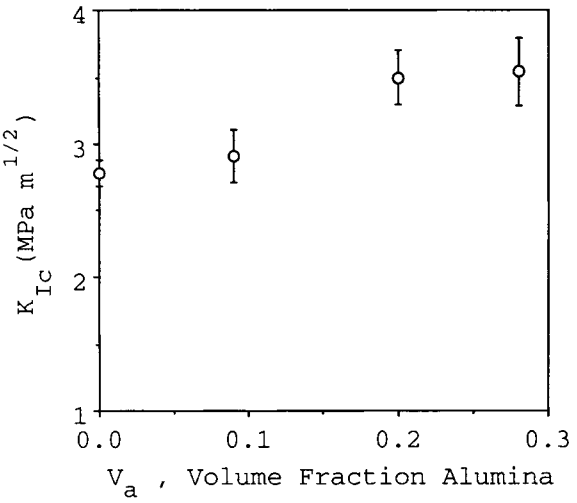

Figure 9 Fracture toughness, K_{Ic}, vs. volume fraction alumina, V_a, for hybrid particle composites containing 15 phe Paraloid KM330 based on DER 664.

alumina ($V_a < 0.1$). The rubber-filled composite, $V_a = 0$, failed by stable crack growth. As the volume fraction of alumina was increased ($0 < V_a < 0.2$), the tendency for initiation type failure increased. That is to say, as the volume fraction of alumina increases in this region, the amount of stable crack growth before failure decreases. Further increases in the concentration of alumina ($V_a > 0.2$) result in a return to the tendency for stable crack propagation. The return to stable crack growth corresponds to relative particle spacing approaching the size of the filler particles and the rise in fracture toughness. Sample casting was not possible for volume fractions of alumina above 0.28. Therefore, the "optimum" hybrid particle composite was taken to be the material containing 28 volume percent alumina (155 phe alumina) and 15 phe Paraloid KM330. Figure 9 shows a K_{Ic} vs. V_a plot for DER 664 hybrid particle composites, a maximum in K_{Ic} vs. V_a was found at 20–28 volume percent alumina filler. The optimum DER 664 hybrid composition was then taken to be 20 volume percent alumina (100 phe alumina) and 15 phe rubber filler.

A summary of the physical properties of the optimized materials is given in Tables I and II. The tables contain fracture toughness, Young's Modulus, E, fracture energy, G_{Ic}, compressive yield strength, σ_{yc}, and glass transition temperature, T_g, data for neat epoxies, rubber-filler optimized composites, and the optimum hybrid particle composites. In general, the addition of rubber filler to neat epoxies results in an increase in fracture toughness, but a decrease in both Young's Modulus and yield strength. On the other hand, a comparison of the hybrid particle composites to the neat materials shows that both fracture toughness and modulus are increased through hybrid particle addition. In addition, hybrid particle-toughened materials have nearly the same yield strength as the neat epoxies.

Hybrid Particle-Toughening and Plastic Zone Effects

Specimens were prepared that contained alumina particle volume concentrations equal to those found in the optimum hybrid particle composites (e.g., 134 phe alumina for DER 661). Likewise, rubber particle-filled resins with the same volume fraction of Paraloid KM330 as the optimum hybrid particle composites were evaluated in the study (e.g., 11 phe Paraloid for DER 661). A summary of the physical properties of modulus, fracture toughness, and yield strength measured for these materials is given in Tables IV and V. In addition, the properties of the neat epoxies, the optimum rubber filled resins, and the optimum hybrid particle composites are tabulated in Tables IV and V.

The critical crack opening displacement, δ_{tc},can be calculated from

$$\delta_{tc} = \frac{K_{Ic}^2}{\sigma_{yt} E} \tag{29}$$

Table IV Estimates of Crack Opening Displacement, δ_{tc}, for DER 661 Matrices

Paraloid (phe)	Alumina (phe)	E (GPa)	K_{Ic} (MPa$\sqrt{m}$)	σ_{yc} (MPa)	δ_{tc} (μm)
0	0	2.7 ± 0.1	0.8 ± 0.1	95 ± 1	3
11	0	2.2 ± 0.1	2.5 ± 0.2	88 ± 2	42
15	0	2.2 ± 0.1	2.6 ± 0.2	71 ± 2	58
0	134	4.9 ± 0.2	1.8 ± 0.2	129 ± 1	7
15	155	3.9 ± 0.3	3.6 ± 0.2	101 ± 1	44

Table V Estimates of Crack Opening Displacement, δ_{tc}, for DER 664 Matrices

Paraloid (phe)	Alumina (phe)	E (GPa)	K_{Ic} (MPa$\sqrt{m}$)	σ_{yc} (MPa)	δ_{tc} (μm)
0	0	2.8 ± 0.1	1.1 ± 0.2†	87 ± 3	7
0	0	2.8 ± 0.1	0.9 ± 0.1*	87 ± 3	5
12	0	2.2 ± 0.2	2.7 ± 0.2	78 ± 1	58
15	0	2.1 ± 0.1	2.8 ± 0.1	67 ± 1	72
0	86	4.8 ± 0.2	1.8 ± 0.2	111 ± 3	8
15	100	3.6 ± 0.2	3.5 ± 0.1	85 ± 2	55

* Denotes arrest value.
† Denotes initiation value.

where σ_{yt} is the tensile yield strength of the material. Equation (26) can be substituted into Eq. (29), resulting in

$$\delta_{tc} = \frac{K_{Ic}^2}{(0.75\sigma_{yc}E)} \tag{30}$$

Equation (30) allows for the estimation of the critical crack opening displacement in terms of compressive yield strength, σ_{yc}. δ_{tc} was estimated for each of the materials listed in Tables IV and V. The greatest crack opening displacements are gained by rubber-toughened composites—indicating the ability of ductile materials to blunt the crack tip. Note that the sharpest crack fronts are predicted for the neat epoxies. The rigid particle-filled composites show crack opening displacements similar to those of the corresponding neat materials. This indicates that crack tip blunting plays a minor role in the toughening of composites containing only alumina particles. Presumably, crack pinning is the dominant fracture mechanism for these rigid particle filled composites. If one compares the optimum hybrid particle composites to the rubber-filled resins that have the same concentration of rubber filler as the hybrid composites, it can be seen that each shows about the same level of critical crack opening displacement. It might be inferred from such a comparison that the hybrid particle composite has retained much of the ability of its rubber filled counterpart to deform plastically in the region around the crack front. Figure 10 is an SEM photograph of the fracture surface of a DER 661 composite containing 134 phe alumina (V_a = 0.28). The photograph shows good adhesion between the epoxy matrix and the alumina filler that results in higher yield strengths than those of corresponding neat epoxies (see Tables IV and V). Finite element analysis predicts that substantial stress is transferred to rigid particles when there is good adhesion between the rigid particles and the matrix.[38–40] The position of greatest stress concentration is located over the poles when the rigid particles are placed in a field of uniaxial tensile stress.[38,39] Therefore, it can be envisioned that the overlap of stress fields results in increased deformation of the matrix material between rigid particles. Further, the presence of rubber particles in the case of hybrid particle composites would be expected to enhance the ability of the matrix to deform locally ahead of the crack front. This would also explain why the more ductile DER 664 network requires lower levels of alumina to reach a maximum value of hybrid toughness. It is presumed that while crack pinning is the dominant mechanism for toughening in alumina-filled epoxies, the rigid particles act to enhance localized plastic deformation between particles in the hybrid particle composites.

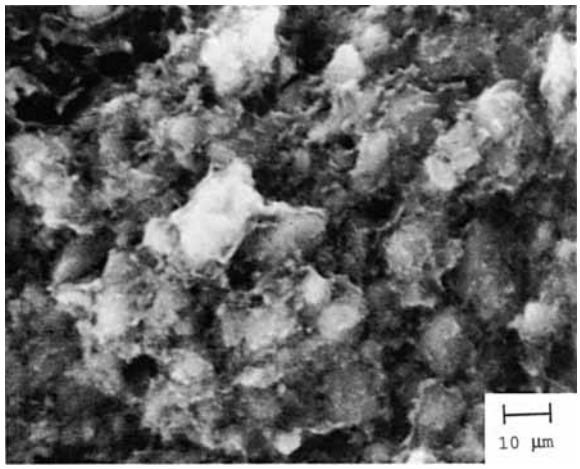

Figure 10 SEM photograph of the fracture surface of a DER 661 composite containing 134 phe alumina.

Table VI Estimate of Plastic Zone Size for Various Matrix Materials

DER/DDS Resin	Paraloid (phe)	K_{Ic} (MPa$\sqrt{m}$)	$2r_p$ (μm)
661	0	0.8	12
661	11	2.5	146
664	0	1.1†	30
664	0	0.9*	21
664	12	2.7	228

* Denotes arrest value.
† Denotes initiation value.

This notion is reinforced when one examines the plastic zone size, $2r_p$, information given in Table VI. The radius of the plastic zone, r_p, for the conditions of plane strain was estimated by Irwin to be[41]

$$r_p = \frac{1}{6\pi}\left(\frac{K_{Ic}}{\sigma_{yt}}\right)^2 \tag{31}$$

where Irwin assumed, for the purposes of analysis, that the plastic zone has a circular cross section. Substituting Eq. (26) into (31) gives

$$r_p = \frac{1}{6\pi}\left(\frac{K_{Ic}}{0.75\sigma_{yc}}\right)^2 \tag{32}$$

which allows the compressive yield strength to be used to estimate the critical size of the plastic zone. The critical size of the plastic zone is given for the neat epoxies in Table VI. In addition, the plastic zone size developed in the rubber-filled specimens with rubber particle concentrations corresponding to those in the optimized hybrid particle composites are given. The average distance separating alumina particles in the hybrid particle composite, d, can be estimated from[42]

$$d = \frac{2D(1 - V_f)}{3V_f} \tag{33}$$

where D is the size of the alumina particles and V_f is the volume fraction of rigid filler in the composite. For A-4000 SG, $D \sim 3.3$ μm. The average distance between alumina particles in the optimized DER 661 hybrid particle composite is approximately 6 μm. For the DER 664 hybrid particle composite, the particle spacing is about 9 μm. Now, consider the case of alumina particle-filled composites that have the same concentration of rigid particles as their optimized hybrid particle composite counterparts. Table VI shows that the size of the plastic zone developed during fracture in the epoxy matrix of these materials is the same magnitude as the alumina particle spacing. Conversely, the plastic zone developed in the epoxy–rubber matrix of optimized hybrid particle composites is much larger than the particle spacing. Crack pinning would, therefore, be less effective in the case of hybrid composites.

Figure 11 is an SEM micrograph of the fractured surface of a hybrid particle filled DER 664 network containing 15 phe Paraloid KM330 and 100 phe alumina. Extensive cavity formation is seen in the fracture surface. Similar cavities were not found on the surface of the alumina filled composites (see Fig. 10). The cavities are attributed, as in the case of rubber-toughened epoxy, to the cavitation and plastic void growth of the rubbery particles.[21–23]

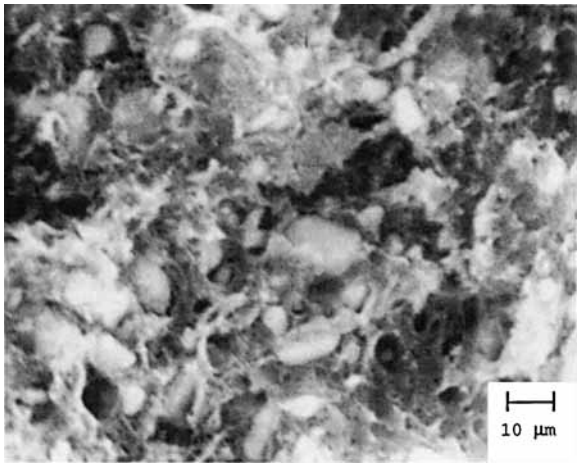

Figure 11 SEM micrograph of the fractured surface of hybrid particle filled DER 664 containing 15 phe Paraloid KM330 and 100 phe A-4000 SG alumina.

CONCLUSIONS

Combinations of rubbery and rigid (hybrid) particles can be used to toughen epoxy resins to an extent greater than either rubbery or rigid particles alone. In this work, an optimized hybrid system gave a sixteen-fold increase in fracture energy in comparison to the corresponding neat network. The use of core-shell rubbery particles allowed for toughening of the resins without alteration of their glass transition temperatures. Optimized hybrid particle composites had greater fracture energies than neat epoxy resins without reduction in important properties such as modulus, yield strength, and glass transition temperature. The rubbery particle-toughening mechanisms of localized shear yielding, cavitation, and plastic void growth are believed to operate in hybrid particle composites. However, a crack front impedance mechanism such as crack pinning operates only in rigid particle filled composites. Hybrid particle composites undergo large-scale plastic deformation in the region around the crack front. It is proposed that well-bonded rigid filler particles, in the case of bulk hybrid particle composites, act as stress concentrators—resulting in greater localized plastic deformation ahead of the crack front than is possible in an equivalently filled rubber particle composite.

Careful consideration of test specimen geometry must be incorporated into evaluation of the fracture properties of toughened glassy polymers. It has been shown that consideration of the geometry of the fracture test specimen plays an important role in the calculation of an appropriate fracture energy for toughened glassy polymers.

The benefits of hybrid particle toughening are expected to be realized when epoxy matrix resins containing optimized blends of dispersed particles are used in fiber reinforced composite laminates. Unidirectional composite laminates offer the opportunity to examine the fracture behavior of hybrid particle matrices in highly constrained geometries without significant alteration of epoxy network reactions. In addition, studies with unidirectional laminates have the potential of revealing important aspects of the interactions between the rubbery and rigid fillers and the epoxy matrix under conditions of failure.

The authors gratefully acknowledge the support of Lord Corporation and Thiokol Corporation. In addition, we appreciate the donation of research materials from Alcoa, Dow Chemical Corporation, and Rohm and Haas Company. We would like to extend special thanks to Dr. K. W. Scott for the many useful and thought provoking discussions regarding the work.

REFERENCES

1. F. J. McGarry, *Proc. R. Soc. Lond.* [*Biol*], **A319,** 58 (1970).
2. A. C. Meeks, *Polymer,* **15,** 675 (1974).
3. C. K. Riew, E. H. Rowe, and A. R. Siebert, in *Toughness and Brittleness of Plastics,* ACS Advances in Chemistry Series 154, R. D. Deanin and A. M. Crugnola, Eds., American Chemical Society, Washington, DC, 1976, p. 326.
4. W. D. Bascom, R. L. Cottington, and C. O. Timmons, *J. Appl. Polym. Sci. Symp.,* **32,** 165 (1977).
5. A. J. Kinloch, S. J. Shaw, and D. A. Tod, in *Rubber-Modified Thermoset Resins,* ACS Advances in Chemistry Series 208, C. K. Riew and J. K. Gillham, Eds., American Chemical Society, Washington, DC, 1984, p. 101.
6. J. Spanoudakis and R. J. Young, *J. Mater. Sci.,* **19,** 473 (1984).
7. A. C. Moloney, H. H. Kausch, T. Kaiser, and H. R. Beer, **22,** 381 (1987).
8. Y. Nakamura, M. Yamaguchi, A. Kitayama, M. Okubo, and T. Matsumoto, *Polymer,* **32,** 2221 (1991).
9. J. D. LeMay, B. J. Swetlin, and F. N. Kelley, in *Characterization of Highly Cross-linked Polymers,* ACS Symposium Series 243, S. S. Labana and R. A. Dickie, Eds., American Chemical Society, Washington, DC, 1984, p. 165.
10. J. D. LeMay and F. N. Kelley, *Adv. Polym. Sci.,* **78,** 115 (1986).
11. J. D. LeMay, doctoral dissertation, University of Akron, 1985.
12. D. L. Hunston, R. J. Moulton, N. J. Johnston, and W. D. Bascom, in *Toughened Composites,* ASTM STP 937, N. J. Johnston, Ed., American Society of Testing and Materials, Philadelphia, 1987, p. 74.
13. W. D. Bascom and D. L. Hunston, in *Rubber-Toughened Plastics,* ACS Advances in Chemistry Series 222, C. K. Riew, Ed., American Chemical Society, Washington, DC, 1989, p. 135.
14. W. L. Bradley, R. N. Cohen, in *Delamination and Debonding of Materials,* ASTM STP 876, W. S. Johnson, Ed., American Society for Testing and Materials, Philadelphia, 1985, p. 389.
15. S. Kunz-Douglass, P. W. R. Beaumont, and M. F. Ashby, *J. Mater. Sci.,* **15,** 1109 (1980).
16. S. C. Kunz, P. W. R. Beaumont, *ibid.,* **16,** 3141 (1981).
17. A. J. Kinloch, S. J. Shaw, D. A. Tod, D. L. Hunston, *Polymer,* **24,** 1341 (1983).
18. A. J. Kinloch, S. J. Shaw, and D. L. Hunston, *ibid.,* **24,** 1355 (1983).
19. A. F. Yee and R. A. Pearson, *J. Mater. Sci.,* **21,** 2462 (1986).
20. *idem, ibid.,* **21,** 2475 (1986).
21. Y. Huang, A. J. Kinloch, *J. Mater. Sci. Lett.,* **11,** 484 (1992).
22. *idem, J. Mater. Sci.,* **27,** 2753 (1992).
23. *idem, ibid.,* **27,** 2763 (1992).

24. F. F. Lange, *Phil. Mag.*, **22,** 983 (1970).
25. A. J. Kinloch, D. Maxwell, and R. J. Young, *J. Mater. Sci.*, **20,** 4169 (1985).
26. J. O. Outwater and D. J. Gerry, *J. Adhesion,* **1,** 290 (1969).
27. J. A. Kies, A. B. J. Clark, in *Fracture—1969,* P. L. Pratt, Ed., Chapman Hall Inc., London, Paper 42, 1969, p. 483.
28. D. P. Williams and A. G. Evans, *J. Testing Eval.*, **1,** 264 (1973).
29. E. R. Fuller, Jr., in *Fracture Mechanics Applied to Brittle Materials,* ASTM STP 678, S. W. Freiman, Ed., American Society for Testing and Materials, Philadelphia, 1979, p. 3.
30. W. C. Young, *Roark's Formulas for Stress and Strain,* Sixth Ed., McGraw-Hill Book Co., New York, 1989, p. 348.
31. P. S. Leevers, *J. Mater. Sci., Lett.,* **5,** 191 (1986).
32. B. Geisler, Doctoral dissertation, University of Akron, 1993.
33. W. C. Young, *Roark's Formulas for Stress and Strain,* Sixth Ed., McGraw-Hill Book Co., New York, 1989, p. 101.
34. J. G. Williams, *Stress Analysis of Polymers,* Halsted Press, New York, 1973, p. 123.
35. J. G. Williams and H. Ford, *J. Mech. Eng. Sci.*, **6,** 405 (1964).
36. ASTM 399–90, *Standard Test Method for Plane-Strain Fracture Toughness of Metallic Materials,* American Society for Testing and Materials, Philadelphia, 1991.
37. A. S. Wronski and M. Pick, *J. Mater. Sci.*, **12,** 28 (1977).
38. B. D. Agarwal, G. A. Panizza, and L. J. Broutman, *J. Am. Ceram. Soc.*, **54,** 620 (1971).
39. F. J. Guild and R. J. Young, *J. Mater. Sci.*, **24,** 298 (1989).
40. S. H. Liu and E. B. Nauman, *ibid.*, **25,** 2071 (1990).
41. J. F. Knott, *Mater. Sci. Eng.*, **7,** 1 (1971).
42. F. F. Lange and K. C. Radford, *J. Mater. Sci.*, **6,** 1197 (1971).

Received October 27, 1993
Accepted March 7, 1994